Clays and Clay Minerals, Vol. 40, No. 6, 707–721, 1992.

AN ELECTRON OPTICAL INVESTIGATION OF ALUMINOSILICATE CEMENTS IN SILCRETES

BALBIR SINGH,[1] R. J. GILKES,[1] AND C. R. M. BUTT[2]

[1] Soil Science and Plant Nutrition, School of Agriculture
The University of Western Australia, Nedlands, W.A. 6009, Australia

[2] CSIRO, Division of Exploration Geoscience, Private Bag
P.O. Wembley, W.A. 6014, Australia

Abstract—Silcretes developed within the *in situ* regolith in the Barr Smith Range, Western Australia, were investigated using optical and electron-beam techniques. One of the cementing agents in these silcretes showed gel-like optical properties and had a variable aluminosilicate chemical composition at the scale of electron microprobe analysis so that it might be considered as allophane-like material. High resolution transmission electron microscopy demonstrated that the material consists of a fine-grained and poorly ordered kaolinite embedded in a matrix of amorphous silica.

Key Words—Amorphous silica, Ion beam thinning, Kaolinite, Silcrete, Transmission electron microscopy.

INTRODUCTION

Silcretes and siliceous duricrusts are common features of arid and semi-arid regions of Australia (Langford-Smith, 1978; Milnes, 1986), South Africa (Summerfield, 1982), Europe, America and other parts of the world (Summerfield, 1983; Kahalf, 1988). Silcrete is a lithological term for a brittle, intensely indurated rock composed mainly of quartz clasts in a matrix of a siliceous cementing agent. Most research on silcretes has been directed to their field distribution (Stephens, 1971), geomorphology (Langford-Smith, 1978; Callen, 1983), petrology (Butt, 1983, 1985) and geochemical characteristics (Milnes and Hutton, 1974, Hutton *et al.*, 1978). Some recent studies (Chadwick *et al.*, 1987a, 1987b; Thiry and Milnes, 1990) have investigated silcretes from a field scale down to the resolution of conventional scanning electron microscopy (SEM). Milnes and Thiry (1992) reviewed current work on silcretes and emphasized the need for use of high resolution techniques to recognize the mechanisms of formation of these materials. Sub-surface silcretes that have developed from dilute groundwaters generally have a distinct mineralogy and morphology and are relatively free of fine-grained components. The resolution provided by SEM and associated electron probe microanalysis (EPMA) is probably sufficient for these silcretes. Pedogenic silcretes and duripans have much more complex morphological, mineralogical and chemical characteristics due to the presence of an intimate mixture of fine-grained phases that cannot always be positively identified by SEM and EPMA. Amorphous silica, opal-CT, cryptocrystalline quartz, clay minerals, carbonates and assemblages of anatase and zircon are common constituents and/or cementing agents of pedogenic silcretes. An initial EPMA study also suggested the occurrence of amorphous aluminosilicate as a cementing agent in highly weathered lateritic profiles of Western Australia (Butt, 1985). This suggestion was supported by observation of the active precipitation of allophane from groundwaters in a broadly similar environment in Western Australia (Thornber *et al.*, 1987). These are novel occurrences since amorphous aluminosilicates typically occur in immature soils developed from volcanic glass (Wada, 1989). The complexity and fine-grained sizes of the cementing phases in these materials warrant the use of high resolution techniques to resolve the composition and to suggest genetic processes involved in the formation of various silcretes.

Chadwick *et al.* (1987a) proposed models for the deposition of various types of silica in soils. According to their model, in loamy soils $Si(OH)_4$ is concentrated in solution due to the high activation energy of Si-O bond breakage. Silica diffuses into the smaller pores from solution and adsorbs onto hydroxyl groups of clay minerals. The adsorbed silica polymers precipitate on drying and shield adsorption sites, thus making adsorption irreversible. The adsorbed silica provides a template for further deposition during the next wetting and drying event, bridging the smaller crevices and pores. According to the model, silica in sandy soils is flocculated from solution and precipitates in the larger voids without preferentially filling the smaller pores. High resolution transmission electron microscopy (HRTEM) can provide direct information to test these and other hypotheses that are based on the particle and void size range, chemical composition, and crystallinity of the fine-grained components of silcretes. In this study, silcretes developed in the *in situ* saprolite and cemented sand horizons of a lateritic profile in the Barr Smith Range, Western Australia, were investigated using analytical transmission electron microscopy (AEM) and HRTEM. The major aim of the study was to in-

vestigate the composition of the silcrete with HRTEM; but low resolution electron-beam techniques, optical microscopy, and X-ray diffraction (XRD) were also used to enable correlation with HRTEM data.

MATERIALS AND METHODS

Samples investigated in this study were taken from the Waterfall profile in the breakaway (erosion scarp) of the Barr Smith Range in Western Australia. This profile is representative of many such breakaways developed on lateritized granitic rocks in western and central Australia and has been described in detail in previous studies (Butt, 1983, 1985). It is exposed in the head of a small gorge cut by a creek flowing westwards over the escarpment. The profile has a vertical face of 7 m (Figure 1), with kaolinitic granite saprolite exposed at the base, passing gradationally upwards to silcrete and sandstone. A near-vertical quartz vein is present at the base of the profile and becomes disorganized upwards, terminating in a stone line about 2.3 m from the top. The profile has importance because the quartz vein demonstrates that the fabric changes below the stone line have taken place *in situ,* in a residual profile. The granitic fabric is perfectly preserved in the saprolite at the base of the profile, with weathered primary minerals represented by clay pseudomorphs and voids and unaltered quartz grains present in their original arrangement. Higher in the profile, where the vein becomes disorganized, the granitic fabric is gradually destroyed and the quartz grains, disaggregated into individual crystals, become more densely packed to develop a grain-supported sandstone fabric (arenose horizon). At the base of the sandstone, there is a thin, discontinuous layer in which the quartz grains have the typical unsupported "terrazzo" (Smale, 1973) or floating fabric (Summerfield, 1983) of silcrete. The saprolite is friable or only weakly cemented; whereas, the sandstone and silcrete are, respectively, moderately and strongly indurated. The silcrete is cemented dominantly by cryptocrystalline quartz and anatase, with detrital zircon (QAZ cement); and the sandstone by the aluminosilicate material under investigation. Samples were taken from the saprolite (#4989), silcrete (#4992) and sandstone (#4993, #4995) within the residual profile adjacent to the quartz vein.

A portion of the friable samples was impregnated with epoxy resin, and polished thin sections mounted on glass slides were made for optical microscopy, EPMA and SEM. The cemented samples were hard enough to allow preparation of petrographic thin sections without impregnation with resin. Freshly exposed fracture and ped surfaces and polished thin sections of the samples were investigated by SEM using a Philips 505 instrument fitted with a backscattered electron (BSE) detector and energy dispersive X-ray analyzer (EDX). Specimens of about 1 cm^3 volume were mounted on aluminium stubs and then coated with carbon and subsequently with a 50 Å thick layer of gold in a vacuum evaporator. Samples for AEM were prepared by two methods. A dilute suspension of a crushed sample was prepared by shaking in distilled water. The <10 μm fraction was separated from the bulk suspension and drops were placed on holey carbon films with a micropipette. The drops were dried under cover at room temperature. Ultrathin sections of cemented samples were prepared by ion milling selected regions removed from petrographic thin sections. All samples for AEM were investigated using a Philips EM 430 instrument operated at 300 kV.

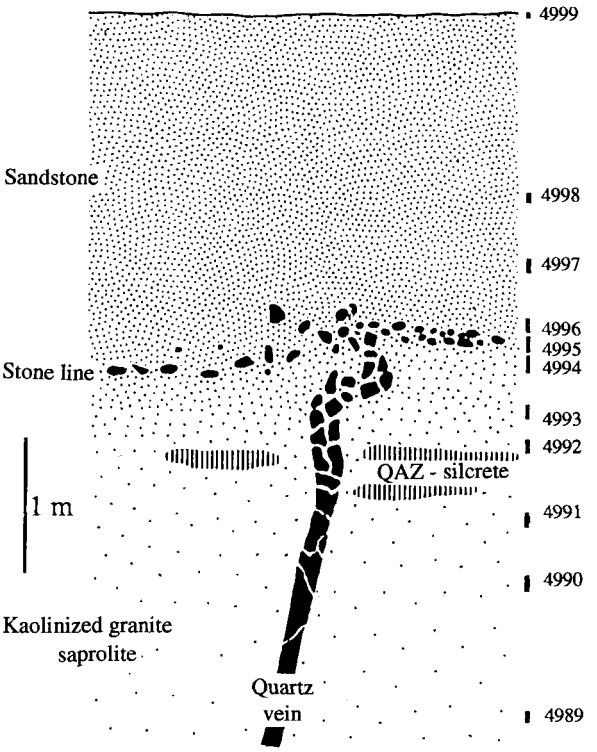

Figure 1. A sketch of Waterfall profile showing position of samples and the quartz vein. Samples number 4989, 4992, 4993, and 4995 were selected for this study because of their *in situ* origin as indicated by the intact quartz vein.

XRD patterns of the whole material and the clay fraction of friable samples were obtained using Cu-Kα radiation with a computer-controlled Philips vertical diffractometer and graphite-diffracted beam monochromator. The digital XRD patterns were interpreted with the aid of XPAS analytical software (Singh and Gilkes, 1992a).

RESULTS AND DISCUSSION

Microfabric and composition of saprolite

A typical optical micrograph of the saprolite (Figure 2) exhibits the preservation of rock fabric by 1) polycrystalline kaolinite pseudomorphs after feldspar crys-

https://doi.org/10.1346/CCMN.1992.0400610 Published online by Cambridge University Press

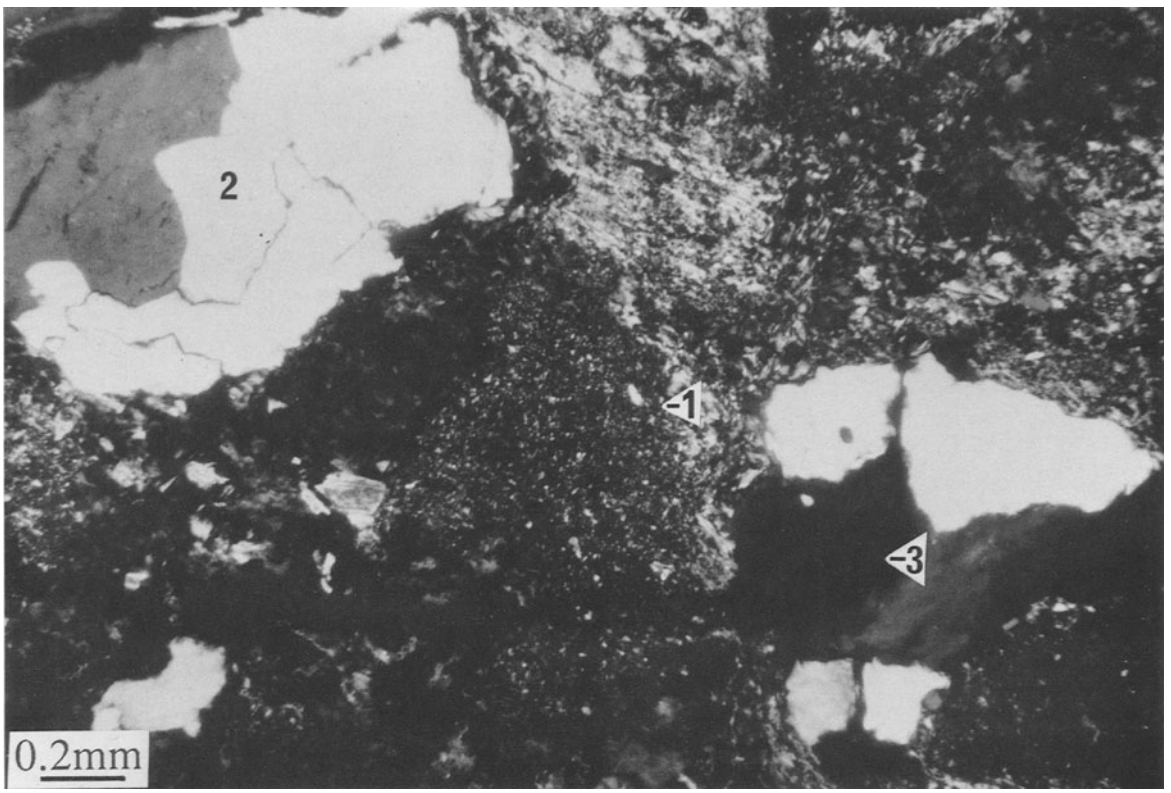

Figure 2. Optical micrograph of saprolite showing 1) kaolinite pseudomorphs after feldspar, 2) large quartz grains that have not separated into subgrains and voids. In 3) an open porous fabric is evident.

tals, 2) quartz, and 3) abundant large voids. Large quartz grains are commonly formed of polycrystalline aggregates. XRD of the bulk material and oriented clay samples showed that quartz and kaolinite are the major crystalline components of the saprolite, which is consistent with the mineralogy of saprolites on felsic rocks in the region. The pseudomorphs of the feldspars are commonly isotropic, either because they consist of randomly oriented arrays of kaolinite crystals (McCrea *et al.*, 1990) or, more probably, because they are partly

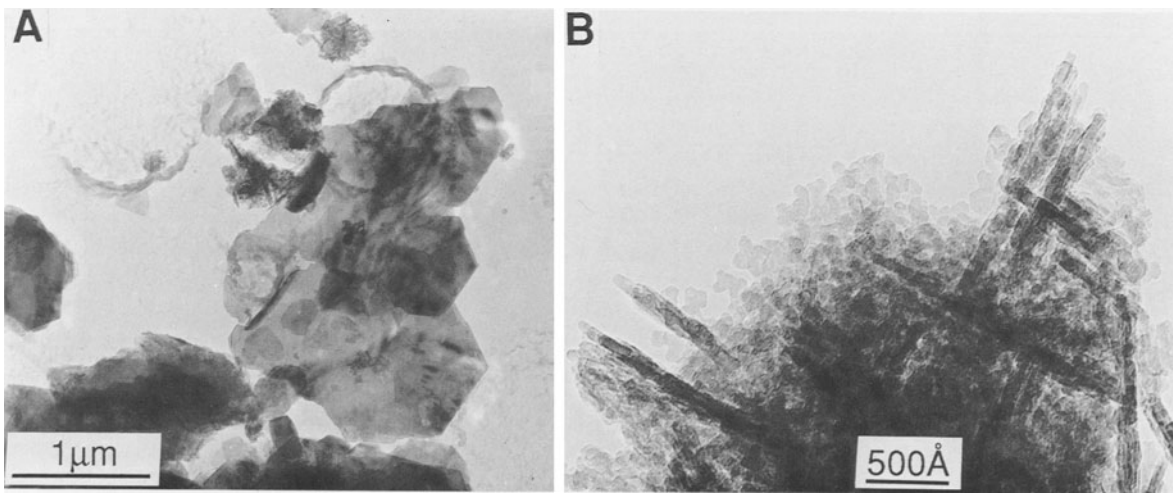

Figure 3. (A) Transmission electron micrograph of a dispersed sample of saprolite material. Euhedral to subhedral hexagonal kaolinite crystals of about 0.5 to 3 μm are the major constituent. (B) Silica grains of about 100 Å diameter, which are combined into rod-shaped particles, are also present.

https://doi.org/10.1346/CCMN.1992.0400610 Published online by Cambridge University Press

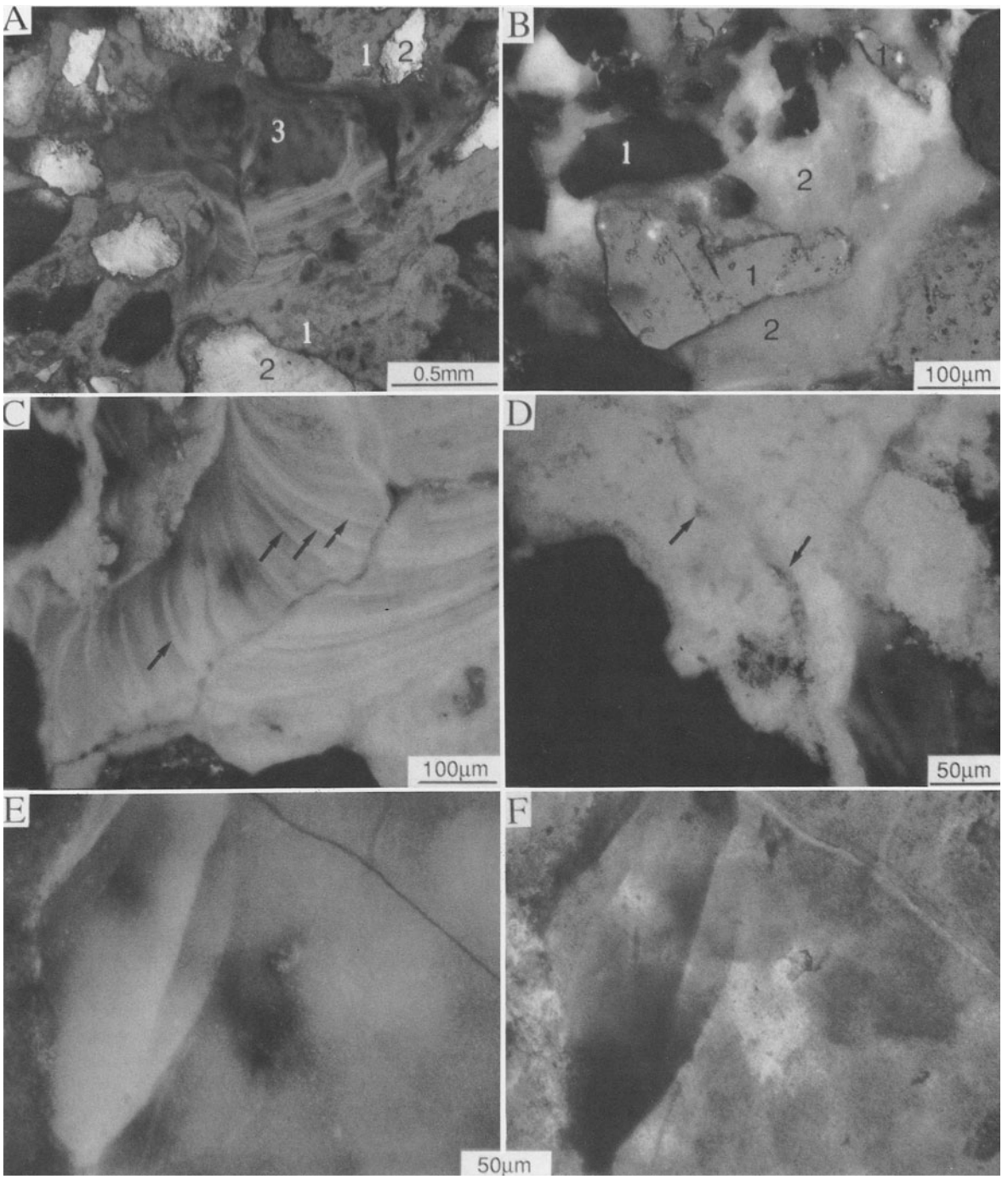

Figure 4. Optical micrographs of silcrete and sandstone samples. (A) Reflected light micrograph of sample #4992 showing 1) QAZ cement adjacent to 2) quartz grains. The voids are filled by 3) an isotropic gel-like aluminosilicate material. The quartz grains have been disrupted but not compacted to a grain supported fabric. (B) Reflected light micrograph of sample #4995. The quartz grains 1) are separated but are more closely packed, and the intergranular space is filled with 2) a gel-like material similar to that in A. (C) A highly magnified view of depositional bands (black arrows) in A. (D) A highly magnified view of QAZ in A. Voids of irregular shape (arrowed) are present. (E) A transmitted light micrograph of the gel-like material in sample #4992. (F) A reflected light magnified view of the gel-like material in sample #4992.

https://doi.org/10.1346/CCMN.1992.0400610 Published online by Cambridge University Press

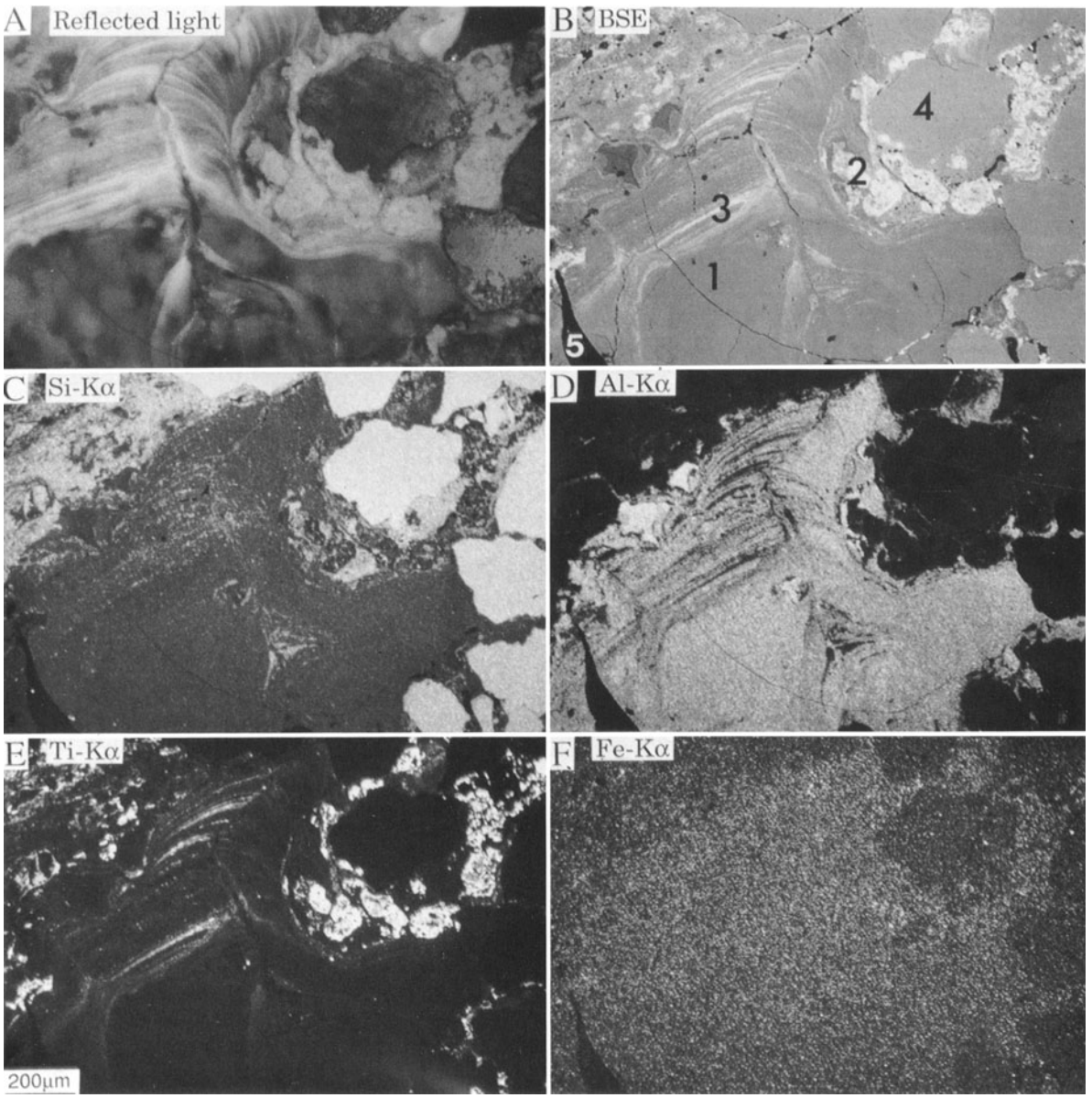

Figure 5. Optical (A) and BSE (B) and X-ray (C–F) images of a region of sample #4992. Quantitative elemental analyses of points 1–5 in Figure 5B are given in Table 1. The X-ray maps show that the gel-like material in (A) is composed of Si, Al, and Ti with a minor content of Fe. The (B) QAZ and (C) depositional bands mainly consist of Si and Ti. The points 4 and 5 correspond to quartz and resin, respectively.

infused by amorphous material. This material is intimately associated with isotropic aluminosilicate cement in adjacent veinlets and is assumed to be similar in composition. The pseudomorphs are very porous and preserve only the external morphology of the parent feldspar grains. Because of the dissimilarity between the structures of the primary feldspar and the secondary kaolinite, topotactic or epitactic alteration is not possible and the kaolinite crystals simply grow (precipitate) in a random orientation from solution (Anand *et al.*, 1985). In contrast pseudomorphs of mica grains are composed of parallel arrays of kaolinite plates, which may be as large as 10 μm, that have formed by topotactic or epitactic replacement of the mica (Gilkes and Suddhiprakarn, 1979; Banfield and Eggleton, 1988; Singh and Gilkes, 1991).

TEM micrographs of <10 μm fraction of saprolite material (#4989) are shown in Figure 3. Euhedral to subhedral hexagonal kaolinite crystals of about 0.5 to 3 μm are the major constituent (Figure 3A). Halloysite, which elsewhere is a common lateritic weathering product of feldspars and mica (McCrea *et al.*, 1990),

https://doi.org/10.1346/CCMN.1992.0400610 Published online by Cambridge University Press

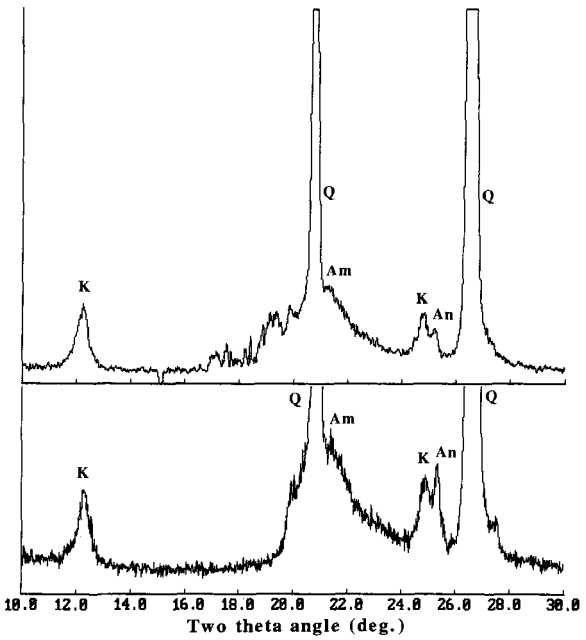

Figure 6. XRD pattern of (A) sample #4992 and (B) #4995. In addition to quartz (Q) amorphous material (Am), kaolinite (K) and anatase (An) are present in both samples. Anatase is present in comparatively greater amount in sample #4992.

Table 1. Table showing the quantitative analysis of points 1–5 marked in Figure 5B.

	1	2	3	4	5
SiO_2	59.98	32.85	50.81	100	0.0
Al_2O_3	22.30	3.62	10.11	0.0	0.0
Fe_2O_3	0.53	0.61	0.39	0.0	0.0
TiO_2	3.49	47.74	23.99	0.0	0.0
Total	86.85	85.21	85.63	100	0.0

is absent in this profile. In addition, a significant amount of fine-grained amorphous silica is present (Figure 3B). The silica grains are anhedral, about 100 Å in diameter and are combined into rod-shaped particles. This occurrence of silica is consistent with many other studies of regolith in arid environments in Australia (e.g., Langford-Smith, 1978) and is in contrast to findings for more humid (>800 mm rainfall) regions of Western Australia where similar granitic saprolites usually contain no secondary silica (Anand *et al.*, 1985; Gilkes and Suddhiprakarn, 1979). The presence of secondary silica is considered to reflect a change from the leaching conditions that prevailed during laterization in the Tertiary to present-day semi-arid to arid regimes (Ollier, 1978; Butt, 1981, 1985).

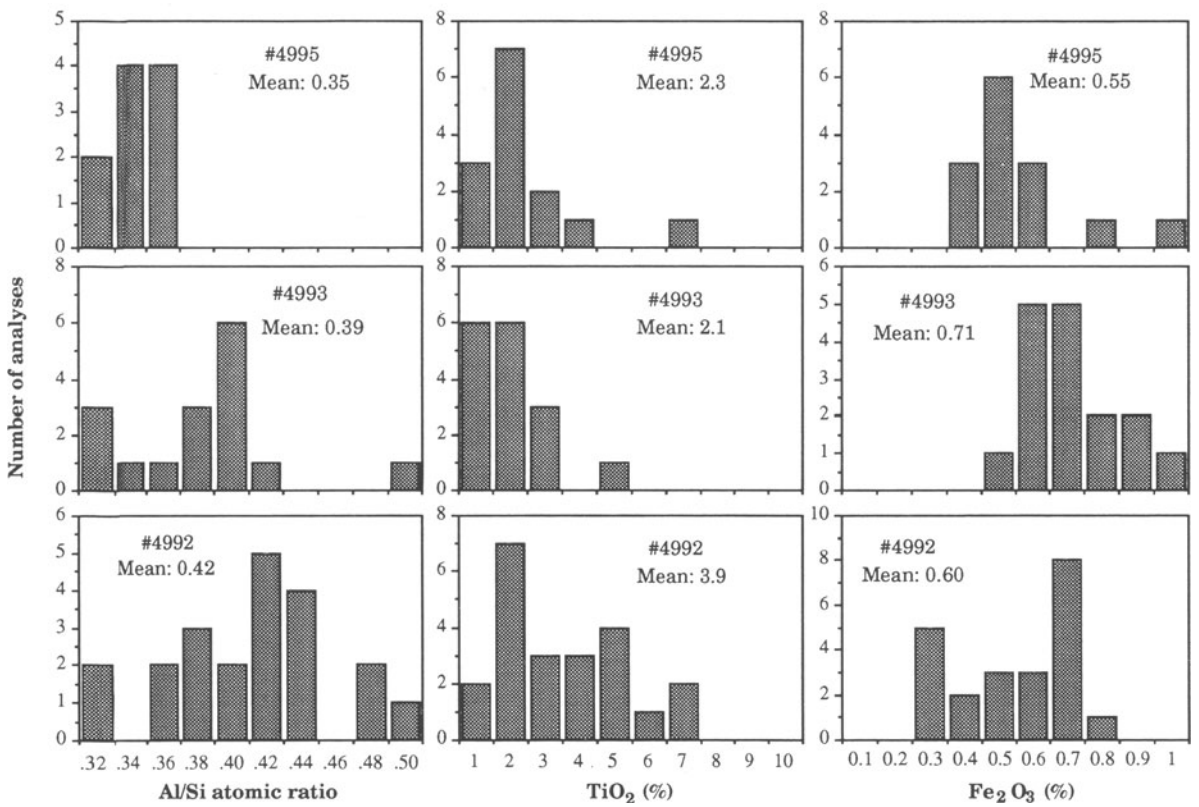

Figure 7. Histograms showing variations in the elemental composition of the aluminosilicate gel-like material determined by EMPA.

https://doi.org/10.1346/CCMN.1992.0400610 Published online by Cambridge University Press

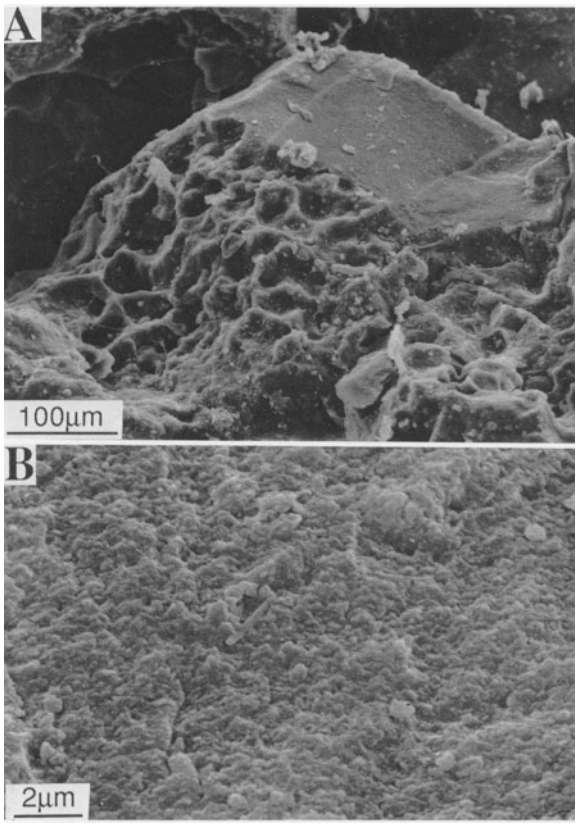

Figure 8. (A) Scanning electron micrographs of a fracture surface of aluminosilicate gel-like material in sample #4993. The fracture surface exhibits regions of concoidal fracture, and ped surface shows a honeycomb morphology that may be indicative of illuviation. (B) A high magnification view of a fracture surface showing fine-grained features.

Microfabric of silcrete

In the arenose horizons of the profile, the distinctive kaolinite pseudomorphs of feldspar are absent, due to eluviation or dissolution (Figure 4). The quartz grains have become disrupted and are more closely packed and the intergranular spaces are partly filled by two types of cement (Butt, 1985):

1) Opaque (transmitted light) or pale yellow (reflected light) granular-textured QAZ cement; and
2) Translucent brown (transmitted light) or white (reflected light) banded, gel-like massive-textured aluminosilicate cement.

The QAZ cement is deposited adjacent to and above the quartz grains and predates the aluminosilicate that infills the voids. It is dominant in the silcrete (#4992), but its abundance decreases sharply upwards. Only small amounts are present in the sandstone (#4995), which is cemented mainly by the aluminosilicate. The terazzo or floating grain fabric of the silcrete is associated with QAZ cement; whereas, the supported grain fabric of the sandstone is associated with gel-like aluminosilicate cement.

X-ray maps for Si, Al, Ti, Fe, and a BSE image are shown in Figure 5. The brightest points in an element map correspond to points of maximum concentration for that particular element. The quantitative elemental composition of the indicated points (1–5) in Figure 5B are given in Table 1 so that the maps may be interpreted semiquantitatively by reference to these quantitative analyses. The X-ray maps show that the QAZ cement is composed mostly of Si and Ti and the aluminosilicate of Si, Al, Ti, and minor Fe. The deposition bands are alternately rich and poor in Ti. XRD of the whole material for two samples (Figure 6) shows that quartz, kaolinite, and anatase are the only crystalline phases present in significant amounts. A broad band centered at 4.1 Å, which resembles the diffraction band of opal-CT (Jones and Segnit, 1971), can also be recognized in XRD patterns for both samples.

Histograms showing the variation in elemental composition, determined by EPMA, of the gel-like aluminosilicate material are shown in Figure 7. Titanium and Fe are present in significant amounts in these materials. The Al/Si atomic ratio increases with depth. There is considerable variability in the Al/Si atomic ratio for the lower horizons, indicating that a mixture of minerals is present, but for sample #4995 the ratio is remarkably uniform. The uniformity in sample #4995 indicates that either the material is single phase or is a mixture with the constituent phases present in constant proportions at a scale much smaller than the spatial resolution of EPMA (~5 μm). Similar uniformity has been noted in aluminosilicate cement from other localities (Butt, 1983). XRD indicates that the aluminosilicate material consists of kaolinite and an amorphous material that is probably opal-CT; but this does not preclude the existence of an amorphous aluminosilicate. It is not possible to determine the relative quantities of the phases by XRD; thus, the Al/Si ratio cannot be calculated and compared with the values determined by EPMA. Therefore, these techniques cannot distinguish if kaolinite is in a very fine-grained mixture with amorphous silica and/or an allophane-like phase.

The morphology of a ped surface coated with aluminosilicate material is shown in Figure 8A. The honeycomb-like morphology is indicative of an illuviated/deposited material and the conchoidal fracture may indicate an amorphous material. A high resolution SEM image of the conchoidal fracture surface (Figure 8B) shows it to have a fine-grained fabric consisting of ~1 μm particles.

High resolution transmission electron microscopy of the aluminosilicate

The gel-like aluminosilicate material was thinned to electron transparency by ion beam thinning to enable

https://doi.org/10.1346/CCMN.1992.0400610 Published online by Cambridge University Press

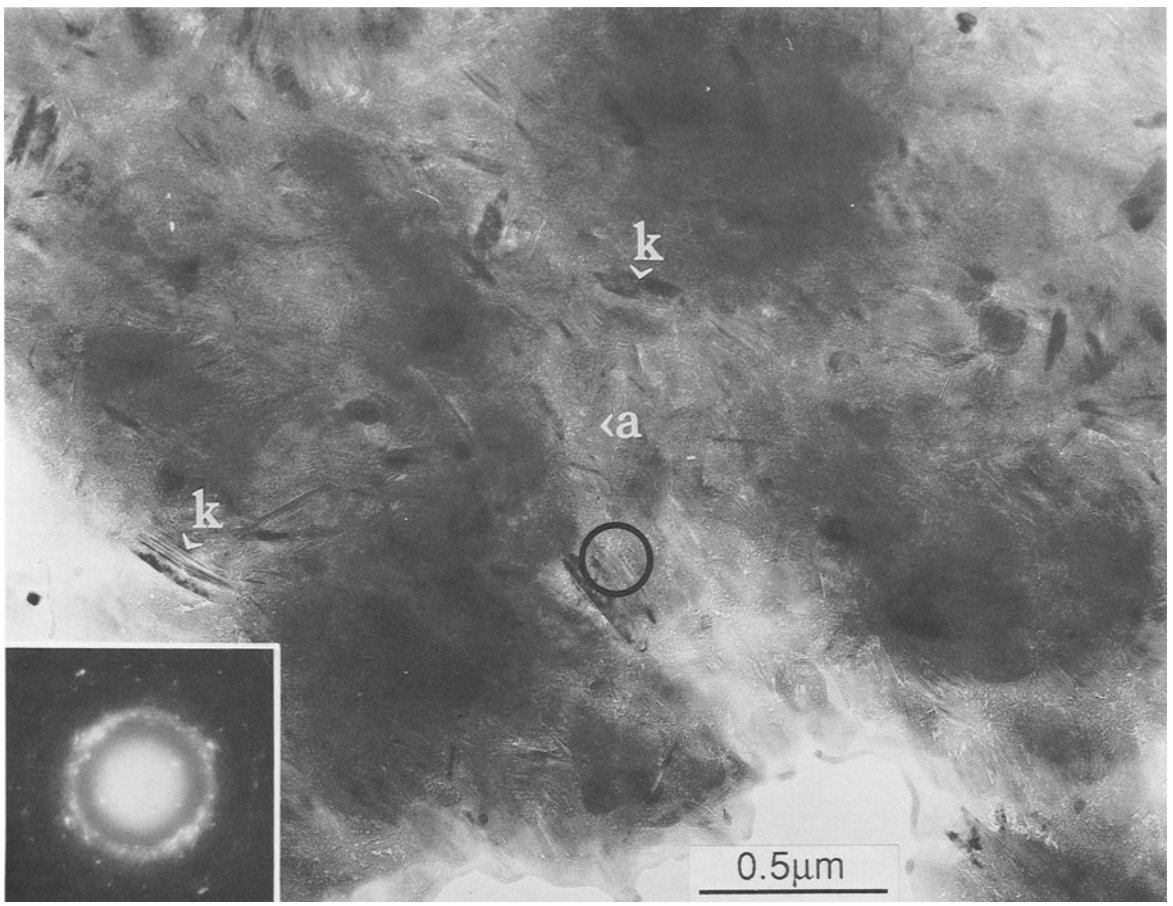

Figure 9. A low magnification TEM micrograph and SAED pattern of aluminosilicate gel-like material. Elongate kaolinite crystals (k) and an amorphous granular material (a) are present.

high resolution AEM studies of the morphology and chemical composition of the constituent phases. A low magnification TEM micrograph and SAED pattern are shown in Figure 9. The material exhibits a complex fabric containing granular and elongate materials with few voids. The SAED pattern consists of reflections for kaolinite and a broad diffraction band centered at about 4.1 Å. The elongate regions represent kaolinite crystals with their (001) plane approximately parallel to the electron beam. These kaolinite crystals are uniformly distributed and randomly oriented in the plane of section, which indicates that they are randomly oriented in three dimensions. The kaolinite crystals not having their (001) plane parallel to the electron beam are present, but they are not as evident due to poor diffraction contrast and the small thickness of the crystals. The broad diffraction band corresponds to the granular regions, which contain very small cavities of irregular shape. Electron diffraction patterns of many areas were compared, showing the intensity of the 4.1 Å diffraction band increased with the increase in proportion of granular material in the selected area. Similarly, convergent beam electron diffraction (CBED) patterns of approximate 30 nm regions also showed that the 4.1 Å band originates from the granular regions. The morphological characteristics of the granular regions are clearly shown in very high resolution images (Figure 10). The diameter of the irregular cavities ranges from about 5–30 nm. The size of continuous amorphous regions ranges from about 10–40 nm.

Chemical composition of the amorphous material

Regions that appeared to be amorphous on the basis of electron diffraction and morphology were analyzed by AEM. The thickness of the ion beam thinned section varied from 10–60 nm, which is similar to the average thickness of amorphous regions and is greater than the size of most kaolinite crystals. Therefore, it is highly probable that regions that appear to be entirely amorphous may have some kaolinite within the thickness of the section. In order to overcome this difficulty, amorphous regions free of kaolinite were located by

https://doi.org/10.1346/CCMN.1992.0400610 Published online by Cambridge University Press

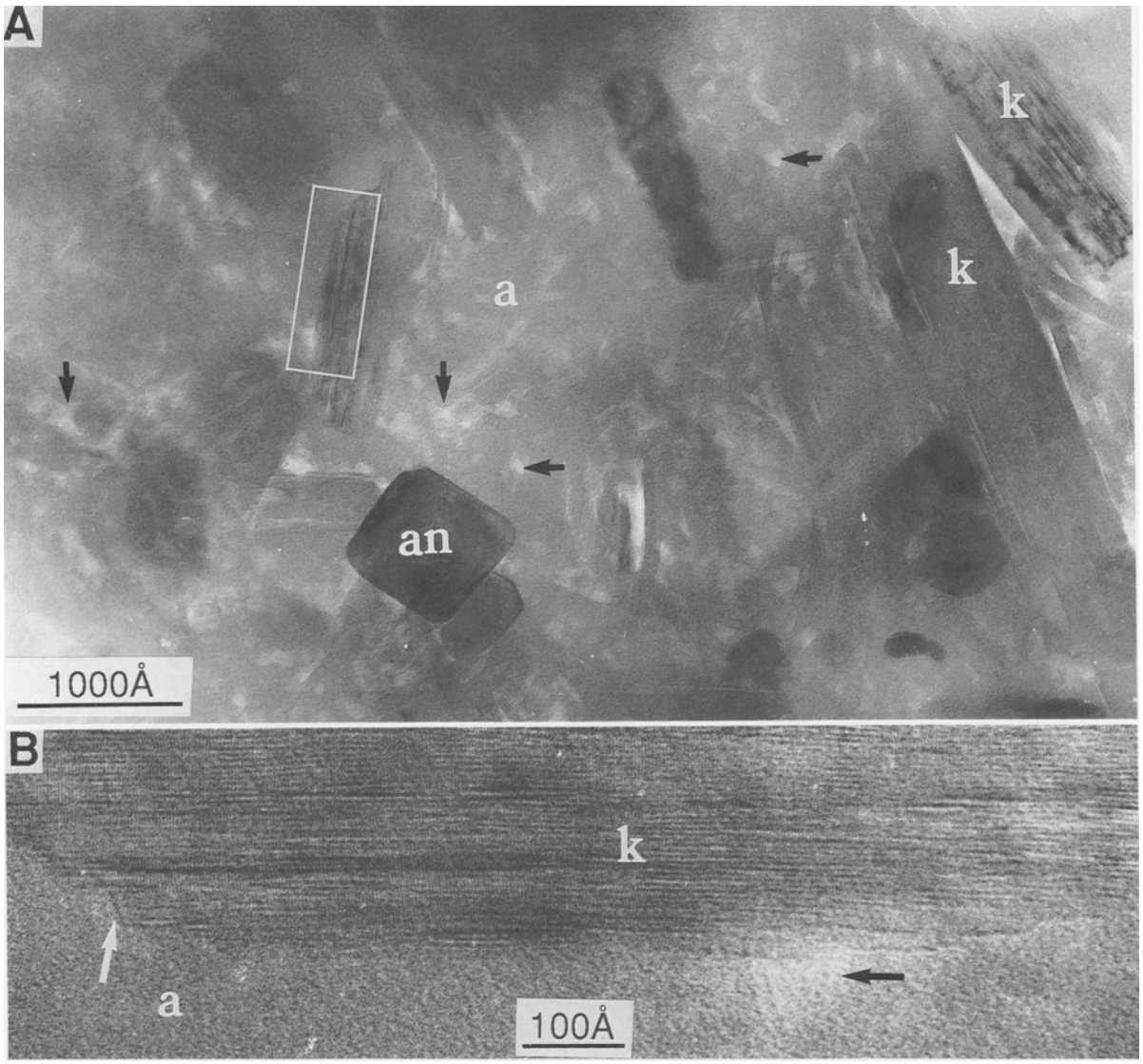

Figure 10. (A) HRTEM micrograph of aluminosilicate gel-like material. Kaolinite (k) and anatase (an) crystals are enclosed in a matrix of amorphous material (a). Cavities of irregular shape and size (black arrows) are present in the amorphous region. (B) A magnified view of the rectangular region marked in A containing a kaolinite crystal.

translating the sample while observing the CBED pattern. The kaolinite crystals decomposed in a few seconds under the converged beam, and the diffraction pattern disappeared. Therefore, only those regions that, during the initial few seconds of observation, produced CBED patterns free of sharp reflections and had a strong diffraction band due to amorphous material were considered to be free of kaolinite. Histograms describing the distribution of values of Si and Al for these regions are shown in Figure 11. Si was the major constituent (mean SiO_2 = 91.5; SD = 5.3), although a relatively minor amount of Al was also present (mean Al_2O_3 = 8.5; SD = 5.3), which is most probably due to the inclusion of some kaolinite in the analyzed region.

Interface between kaolinite and the amorphous material

The spatial relationship between kaolinite crystals and the surrounding amorphous material in the gel-like material is clearly seen in Figure 12. The amorphous material contains abundant vesicular voids that may have formed as an initial gel dehydrated. In many regions, the amorphous material was not present in the cavities between adjacent kaolinite crystals, and there were gaps between the kaolinite surface and the surrounding amorphous material (Figures 10A and 12). These features may indicate that the amorphous material invaded pre-existing kaolinite in voids in the

https://doi.org/10.1346/CCMN.1992.0400610 Published online by Cambridge University Press

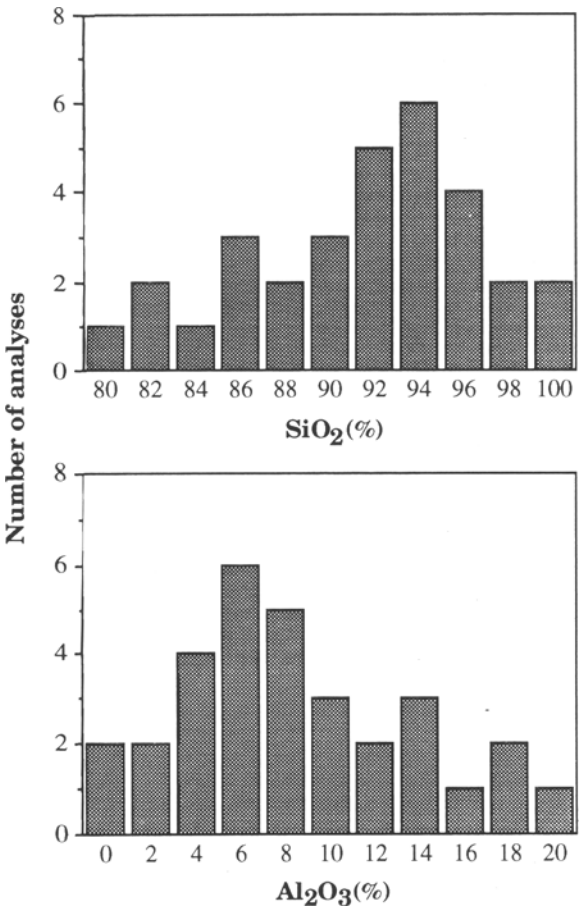

Figure 11. Histograms showing amounts of Si and Al in the amorphous gel-like material.

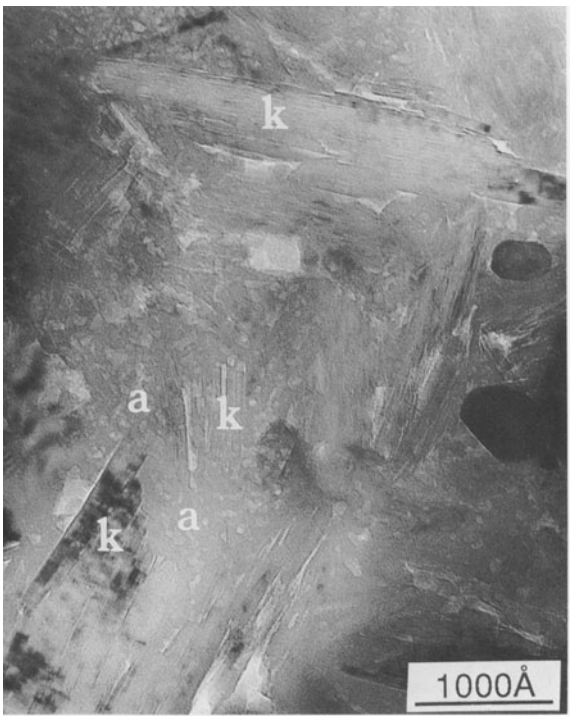

Figure 12. A high contrast TEM micrograph showing (a) amorphous siliceous material filling the space between (k) kaolinite crystals.

sandstone in the form of particles that were too large to penetrate small cavities (Chadwick *et al.*, 1987a). Alternatively, these gaps may be due to contraction as the amorphous material formed by dehydration of an initial gel. In other areas of the section, the amorphous material and kaolinite crystals are in contact at the scale of resolution of the technique (~5 Å), which is demonstrated by kaolinite lattice fringes in immediate contact with the amorphous matrix in Figure 10B.

Properties of the kaolinite crystals

The lattice fringe images for the basal planes of kaolinite within the gel-like aluminosilicate material show that various degrees of structural disorder are present. Figure 13A shows a lattice fringe image of a comparatively well-ordered kaolinite crystal. Large regions showing coherent fringes that are uniform in spacing and contrast are present. The coherent regions are connected by continuous but slightly curved layers, and strain contrast is evident between adjacent coherent regions. The width of coherent regions (marked by white arrows in Figure 13A) ranges from a few to more than 30 layers, and the length of these regions is generally several hundred Å units. Extensive layer bending and terminations are absent. Although some defects are present, the crystals represented by this micrograph may be considered well-ordered kaolinites.

A typical lattice fringe image of a comparatively disordered kaolinite crystal, the most common form of kaolin in the gel-like aluminosilicate material, is shown in Figure 13B. Edge dislocations defined by layer termination are abundant, and individual layers curve and change contrast over short distances due to varying orientations of the layers. In consequence, regularly ordered, coherently diffracting regions are small and isolated. A remarkable observation in this example is that all layer terminations are in the same direction (left to right in Figure 13B). These layer terminations result in extensive *c*-axis disorder in comparison to cooperative layer termination that would produce only localized disorder. Some mostly well-ordered kaolinite crystals were found to contain packets of poorly ordered material (Figure 14A). These packets are probably not due to beam damage as layers of ordered kaolinite curve around them. Moreover, their thin lenticular shape is not consistent with beam damage. Another notable observation is that some kaolinite crystals showed splitting of layers (Figure 14B) to form platy voids of about 100 Å width and 7 Å height.

https://doi.org/10.1346/CCMN.1992.0400610 Published online by Cambridge University Press

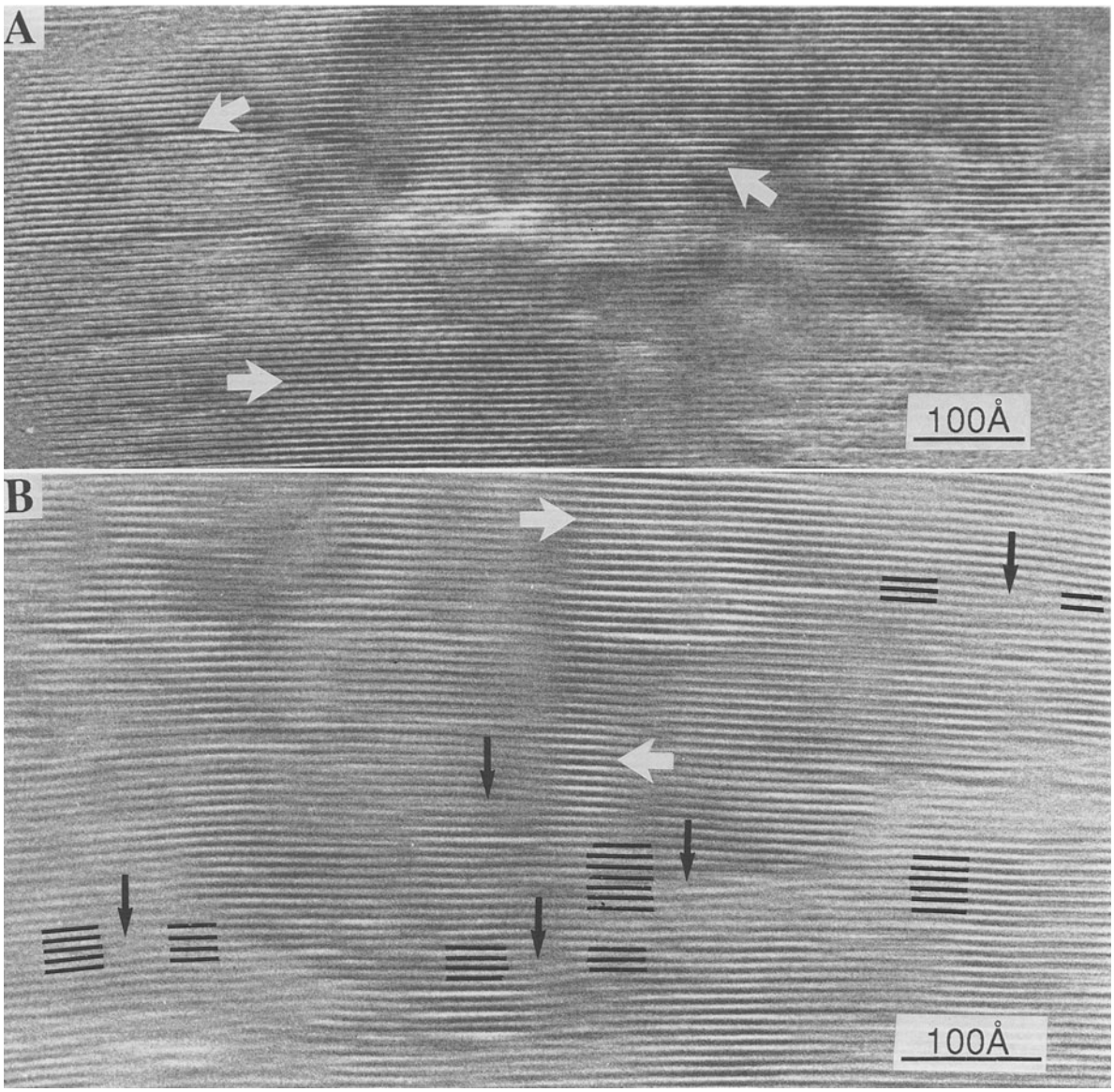

Figure 13. Lattice fringe images for the basal planes of kaolinite crystals contained within the aluminosilicate gel-like material. (A) Large regions (>30 layers) showing coherent 7 Å fringes (indicated by white arrows) that are uniform in spacing and contrast. (B) Lattice fringe image of a disordered kaolinite crystal showing a high density of layer terminations (black arrows); consequently, regular regions are small and isolated.

Layer terminations similar to those shown in Figure 13B have been observed in smectite (Ahn and Peacor, 1986; Klimentidis and Mackinnon, 1986) and illite developed from smectite (Ahn and Peacor, 1986). It is possible that these layer terminations are the markers of arrested or active reactions in which the terminating layers are either growing or more probably shrinking (Veblen, 1983). The discontinuity in the structure at the point of layer termination may serve as channel for transport of ions in solution. This mechanism of ion transport has been considered to be active in many mineral alteration processes (Veblen and Buseck, 1980; Yau *et al.*, 1984; Singh and Gilkes, 1991) that involve gain or loss of ions at a weathering front progressing along a single layer. Thus, these very small and disordered kaolinite crystals may be the residues of the much larger and more highly ordered kaolinite that occurs in saprolite. It is impossible to distinguish this explanation for layer terminations in kaolinite from the possibility that the terminations in kaolinite formed during initial crystal growth and became inactive once embedded in the surrounding layers. This direct observation of defects is consistent with some of the bulk properties of kaolinite. For example, Plançon and

https://doi.org/10.1346/CCMN.1992.0400610 Published online by Cambridge University Press

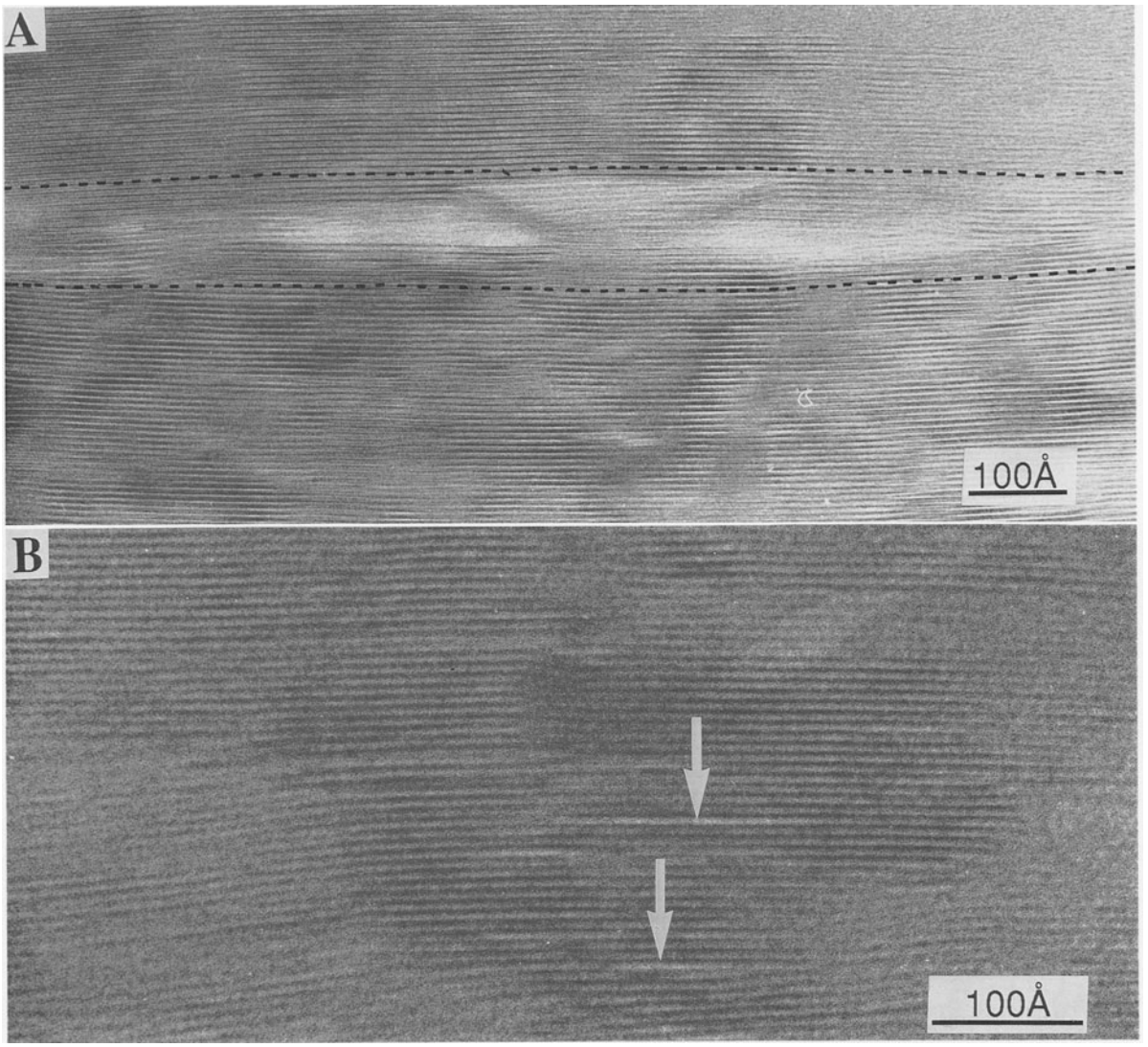

Figure 14. (A) Lattice fringe image of a large ordered kaolinite crystal containing a packet of poorly ordered layers. (B) Lattice fringe image showing incipient exfoliation indicated by the localized expansion of interlayer space to give approximately 100 Å × 7 Å voids.

Tchoubar (1977) pointed out that d(001) calculated from hkl reflections is always 7.15 Å for well-ordered kaolinite, but the spacing of the (001) reflection reaches 7.2 Å or even higher values for disordered kaolinites. It appears that the 7.15 Å spacing originates from the coherent regions that have uniform spacing and the larger 001 spacing is due to the increase in layer spacing at terminations and layer splitting defects. These defects also indirectly increase the observed 001 spacing (by XRD) by decreasing the size of coherently diffracting regions, resulting in broad, displaced reflections (Trunz, 1976).

Thickness and width of a large number of kaolinite crystals in the gel-like material were measured from micrographs and population statistics determined (Figure 15). The width of kaolinite crystals ranged from 0.05 to 0.5 μm with a median value of 0.15 μm, which is similar to that of kaolinite in surface soils in the region. Singh and Gilkes (1992b) measured crystal widths for 8 soil kaolinites from southwestern Australia. The median value ranged from 0.06 to 0.12 μm for soil kaolinites in comparison to 0.28 μm for a reference Georgia kaolinite. The microstructural relationships between kaolinite and amorphous material described above do not clearly indicate whether or not the kaolinite formed from an amorphous aluminosilicate phase. Crystallization of layer silicates from an amorphous phase has been shown to proceed via the formation of hollow bubbles that become coated with layers of the clay minerals (Parfitt and Henmi, 1980;

https://doi.org/10.1346/CCMN.1992.0400610 Published online by Cambridge University Press

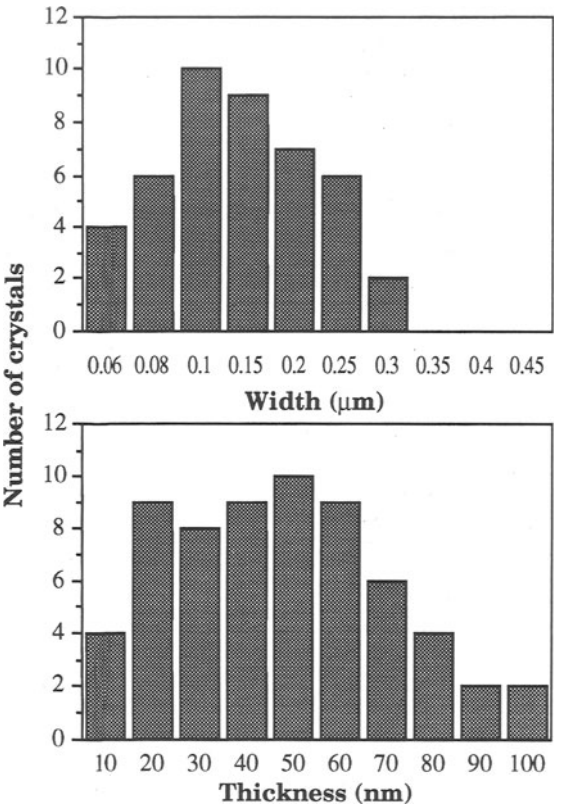

Figure 15. Histograms showing the dimensions of kaolinite crystals measured from TEM micrographs.

Eggleton, 1987). No such structures or any other intermediary morphology or phase (e.g., smectite) suggestive of formation of kaolinite by segregation from an initial amorphous aluminosilicate were observed. The crystal dimensions and disordered nature of this kaolinite are similar to these properties for soil kaolinites and it appears that in the gel-like material kaolinite crystals have become simply embedded in a siliceous matrix.

Mechanisms of silcrete formation

The Waterfall profile exhibits a progressive upward change from dominantly kaolinitic saprolite to the cemented quartz-rich arenose horizon near the surface. This change occurred *in situ,* without either erosional or depositional events, and was brought about by the removal of kaolinite, vertical settling and compaction of quartz grains, and introduction of QAZ and aluminosilicate cements. This evolution involved at least three chemical stages.

Stage 1: Removal (dissolution) of much kaolinite. There is no petrographic evidence for eluviation such as cutans or an illuviated clay horizon; therefore, it is presumed that the kaolinite was dissolved, and the process facilitated by the high porosity of the pseudomorphs after feldspars. No hydrous Al oxides (e.g., gibbsite, boehmite) are present in any horizon, which indicates that the kaolinite dissolved congruently under conditions in which these oxides are unstable. Congruent dissolution of kaolinite occurs below pH 5.0, becoming significant below pH 4.0 (Norton, 1973). Such low pH values are consistent with weathering of poorly buffered kaolinitic saprolite under the humid conditions prevailing in this region in the past.

Stage 2: Introduction and precipitation of QAZ cement. The intimate association of quartz and anatase in QAZ cement implies that solution, migration and precipitation of Si and Ti took place together. Titanium mobilization occurs below pH 4.0 (Baes and Mesmer, 1976). Similar conditions could also release silica by dissolution of quartz, kaolinite and zircon, as evident from the presence of skeleton relicts in the cement. Some quartz and anatase are assumed to have precipitated from solution or a colloidal sol, possibly with some expansive growth resulting in the unsupported "terrazo" fabric. This precipitation must have postdated and terminated the mechanical activity associated with the collapse of the quartz vein and the settling of the quartz grains forming the arenose horizon. It is suggested that silcrete formation occurred under less humid or at least more marked seasonal climate than those prevailing during kaolinite dissolution.

Stage 3: Introduction and precipitation of aluminosilicate cement. This probably occurred during a late stage in the evolution of the profile, associated with reduced leaching due to aridity. The data presented indicate that the aluminosilicate cement consists of very small kaolinite crystals uniformly distributed in opaline silica. The kaolinite may be neoformed, rather than mechanically derived from the saprolite. The silica was probably initially formed as opal-A which then altered to opal-CT on ageing and dehydration. The irregular shapes and sizes of the cavities that are a feature of this material may be due to shrinking associated with partial dehydration and structural ordering of the opal-A to opal-CT (Senkayi *et al.,* 1985; Jones and Segnit, 1971). The data do not, however, give unequivocal evidence as to the origin of the kaolinite or the nature of cement when it was introduced. Possible mechanisms include:

1) Introduction and precipitation of amorphous aluminosilicate material that then transformed to opal-A and kaolinite;
2) Deposition of opal-A and kaolinite from a silica-rich solution that carried kaolinite in suspension. The mechanism of formation of this kaolinite is unknown, but precipitation from an aluminosilicate precursor is possible.
3) Introduction of silica into neoformed kaolinite occupying the intergranular voids of the sandstone.

https://doi.org/10.1346/CCMN.1992.0400610 Published online by Cambridge University Press

Alternatively, these kaolinite crystals may be the partly dissolved and structurally disordered residues of the much larger and more perfectly ordered kaolinite crystals that occur in saprolite.

SUMMARY

The gel-like aluminosilicate material is composed of very fine-grained kaolinite and amorphous silica which are almost homogeneously mixed at a sub-micron scale. The gel-like optical properties and almost uniform aluminosilicate composition determined by EPMA are due to the homogeneous mixture of fine-grained (<0.5 μm) kaolinite with amorphous silica. There is no evidence for the presence of allophane or imogolite-like compounds. This study has clearly highlighted the essentiality of high resolution techniques to resolve the composition of fine-grained materials in soils and other regolith materials.

REFERENCES

Ahn, J. H. and Peacor, D. R. (1986) Transmission and analytical electron microscopy of the smectite-to-illite transition: *Amer. Mineral.* **72,** 353–356.

Anand, R. R., Gilkes, R. J., Armitage, T. M., and Hillyer, J. W. (1985) Feldspar weathering in a lateritic saprolite: *Clays & Clay Minerals* **33,** 31–43.

Baes, C. F. and Mesmer, R. E. (1976) *The Hydrolysis of Cations:* John Wiley, New York.

Banfield, J. F. and Eggleton, R. A. (1988) Transmission electron microscope study of biotite weathering: *Clays & Clay Minerals* **36,** 47–60.

Butt, C. R. M. (1981) The nature and origin of the lateritic weathering mantle, with particular reference to Western Australia: in *Geophysical Prospecting in Deeply Weathered Terrain,* H. A. Doyle, J. E. Glover, and D. I. Groves, eds., University of Western Australia, Geol. Dept. and Extension Service, Publ., **6,** 11–29.

Butt, C. R. M. (1983) Aluminosilicate cementation of saprolite, grits and silcretes in Western Australia: *J. Geol. Soc. Aust.* **30,** 179–186.

Butt, C. R. M. (1985) Granite weathering and silcrete formation on the Yilgarn Block, Western Australia: *Aust. J. Earth Sci.* **32,** 415–432.

Callen, R. A. (1983) Late Tertiary "grey billy" and the age and origin of surfacial silicification (silcrete) in South Australia: *J. Geol. Soc. Aust.* **30,** 393–410.

Chadwick, O. A., Hendricks, D. M., and Nettleton, W. D. (1987a) Silica in Duric soils: I. A depositional model: *Soil Sci. Soc. Am. J.* **51,** 975–982.

Chadwick, O. A., Hendricks, D. M., and Nettleton, W. D. (1987b) Silica in duric soils: II. Mineralogy: *Soil Sci. Soc. Am. J.* **51,** 982–985.

Eggleton, R. A. (1987) Noncrystalline Fe-Si-Al-oxyhydroxides: *Clays & Clay Minerals* **35,** 29–37.

Gilkes, R. J., Anand, R. R., and Suddhiprakarn, A. (1986) How the microfabric of soils may be influenced by the structure and chemical composition of parent minerals: in *Trans. Int. Soil Sci. Conf. Hamburg* **6,** 1093–1106.

Gilkes, R. J., Scholz, A., and Dimmock, G. M. (1973) Lateritic deep weathering of granite: *J. Soil Sci.* **24,** 523–536.

Gilkes, R. J. and Suddhiprakarn, A. (1979) Biotite alteration in deeply weathered granite. II. The oriented growth of secondary minerals: *Clays and Clay Minerals* **27,** 361–367.

Hutton, J. T., Twidale, C. R., and Milnes, A. R. (1978) Characteristics and origin of some Australian silcretes: in *Silcrete in Australia,* T. Langford-Smith, ed., University of New England, Armidale, Australia.

Jones, J. B. and Segnit, E. R. (1971) The nature of opal. I. Nomenclature and constituent phases: *J. Geol Soc. Aust.* **18,** 57–68.

Kahalf, F. I. (1988) Petrography and diagenesis of silcrete from Kuwait, Arabian Gulf: *J. Sed. Petrol.* **58,** 1014–1022.

Klimentidis, R. E. and Mackinnon, I. D. R. (1986) High-resolution imaging of ordered mixed-layer clays: *Clays & Clay Minerals* **34,** 155–164.

Langford-Smith, T. (1978) *Silcretes in Australia:* Monogr. Ser., Dept. Geography, University of New England, Armidale, Australia.

McCrea, A. F., Anand, R. R., and Gilkes, R. J. (1990) Mineralogical and physical properties of lateritic pallid zone materials developed from granite and dolerite: *Geoderma* **47,** 33–57.

Milnes, A. R. (1986) Armoured landscapes: *Geology Today,* 73–74.

Milnes, A. R. and Hutton, J. T. (1974) The nature of microcryptocrystalline titania in 'silcrete' skins from the Beda Hill area of South Australia: *Search* **5,** 153–154.

Milnes, A. R., and Thiry, M. (1992) Silcretes: in *Weathering Soils and Paleosols,* I. P. Martini and W. Chesworth, Eds., Elsevier, Amsterdam.

Norton, S. A. (1973) Laterite and bauxite formation: *Econ. Geol.* **68,** 353–361.

Ollier, C. D. (1978) Early landform evolution: in *Australia, a Geography,* J. N. Jeans, ed., Sydney University Press, Sydney.

Parfitt, R. L. and Henmi, T. (1980) Structure of some allophanes from New Zealand: *Clays & Clay Minerals* **28,** 285–294.

Plançon, A. and Tchoubar, C. (1977) Determination of structural defects in phyllosilicates by X-ray diffraction. Part II. Nature and proportions of defects in natural kaolinites: *Clays & Clay Minerals* **25,** 436–450.

Senkayi, A. L., Dixon, J. B., Hossner, L. R., Yerima, B. P. K., and Wilding, L. P. (1985) Replacement of quartz by opaline silica during weathering of petrified wood: *Clays & Clay Minerals* **33,** 525–531.

Singh, Balbir and Gilkes, R. J. (1991) Weathering of chromian muscovite to kaolinite: *Clays & Clay Minerals* **39,** 571–579.

Singh, Balbir and Gilkes, R. J. (1992a) XPAS: An interactive computer program for analysis of powder X-ray diffraction patterns: *Powder Diffraction* **7,** 6–10.

Singh, Balwant and Gilkes, R. J. (1992b) Properties of soil kaolinites from south-western Australia: *J. Soil Sci.* (in press).

Smale, D. (1973) Silcretes and associated silica diagenesis in southern Africa and Australia: *J. Sed. Petrol.* **43,** 1077–1089.

Stephens, C. G. (1971) Laterite and silcrete in Australia: A study of the genetic relationship of laterite and silcrete and their companion materials, and their collective significance in the formation of the weathered mantle, soils, relief and drainage of the Australian continent: *Geoderma* **5,** 5–52.

Summerfield, M. A. (1982) Distribution, nature and probable genesis of silcrete in arid and semi-arid southern Africa: in *Aridic Soils and Geomorphic Processes,* D. H. Yallon, ed., Catena Suppl. **1,** 37–65.

Summerfield, M. A. (1983) Silcrete: in *Chemical Sediments and Geomorphology,* A. S. Goudie and K. Pye, eds., Academic Press, London, 59–91.

Thiry, M. and Milnes, A. R. (1990) Pedogenic and groundwater silcretes at Stuart Creek opal field, South Australia: *J. Sed. Petrol.* **61,** 111–127.

Thornber, M. R., Bettenay, E., and Russell, W. G. R. (1987)

A mechanism of aluminosilicate cementation to form a hardpan: *Geochim. Cosmochim. Acta* **51,** 2303–2310.

Trunz, V. (1976) The influence of crystallite size on the apparent basal spacings of kaolinite: *Clays & Clay Minerals* **24,** 84–87.

Veblen, D. R. (1983) Microstructures and mixed layering in intergrown wonestie, chlorite, talc, biotite and kaolinite: *Amer. Mineral.* **68,** 566–580.

Veblen, D. R. and Buseck, P. R. (1980) Chain-width order and disorder in biopyriboles: *Amer. Mineral.* **64,** 687–700.

Wada, K. (1989) Allophane and imogolite: in *Minerals in Soil Environments,* J. B. Dixon and S. B. Weed, eds., Soil Science Soc. America, Madison, Wisconsin.

Yau, Y. C., Anovitz, L. M., Essene, E. J., and Peacor, D. R. (1984) Phlogopite-chlorite reaction mechanisms and physical conditions during retrograde reaction in the marble formation, Franklin, New Jersey: *Contrib. Mineral. Petrol.* **88,** 299–308.

(Received 3 April 1992; accepted 14 September 1992; Ms. 2208)